Bull. Mater. Sci., Vol. 24, No. 2, April 2001, pp. 173–180. © Indian Academy of Sciences.

Particle fracture and plastic deformation in vanadium pentoxide powders induced by high energy vibrational ball-mill

PARTHA CHATTERJEE, S P SEN GUPTA* and SUCHITRA SEN†

Indian Association for the Cultivation of Science, Jadavpur, Kolkata 700 032, India
†Central Glass and Ceramic Research Institute, Jadavpur, Kolkata 700 032, India

Abstract. An X-ray powder profile analysis in vanadium pentoxide powder milled in a high energy vibrational ball-mill for different lengths of time (0–250 h), is presented. The strain and size induced broadening of the Bragg reflection for two different crystallographic directions ([001] and [100]) was determined by Warren–Averbach analysis using a pattern-decomposition method assuming a Pseudo–Voigt function. The deformation process caused a decrease in the crystallite size and a saturation of crystallite size of ~ 10 nm was reached after severe milling. The initial stages of milling indicated a propensity of size-broadening due to fracture of the powder particles caused by repeated ball-to-powder impact whereas with increasing milling time microstrain broadening was predominant. WA analysis indicated significant plastic strain along with spatial confinement of the internal strain fields in the crystallite interfaces. Significant strain anisotropy was noticed in the different crystallographic directions. A near-isotropy in the crystallite size value was noticed for materials milled for 200 h and beyond. The column-length distribution function obtained from the size Fourier coefficients progressively narrowed down with the milling time.

Keywords. X-ray diffraction; ball-milling; plastic deformation; microstrain.

1. Introduction

Vanadium pentoxide is of current interest as an oxidation catalyst and as a thermally-activated electrical and optical switching material. At room temperature, the material is a wide band-gap semiconductor with an orthorhombic lattice. It consists of a number of oxides and suboxides such as VO, V_2O_3, VO_2, V_4O_9, V_2O_5, $V_{2n}O_{5n-2}$ and V_nO_{2n-1}. Most of these compounds exhibit the metal–insulator transition (MIT) which occurs over a wide range of the transition temperature depending on the O/V ratio. Vanadium pentoxide which is the most stable compound of the V–O system also shows a MIT at 257·5°C but is usually regarded as a semiconductor. Nanostructured materials have wider application for their exceptional properties with respect to their bulk counterpart. Recently high-energy vibrational ball-milling has been accepted as a promising method to form nanocrystalline materials. Most of the work in V_2O_5 is limited to nanostructures in two dimensional thin film form (Rubin Aita *et al* 1986; Yong-Su *et al* 1992). In this paper, we have concentrated on the nanostructure that was developed in three-dimensional form i.e. in powder form by high-energy vibrational ball-milling.

The structure of V_2O_5 is unusual and consists of distorted trigonal bipyramids of VO_5 units sharing edges with other units to form zig-zag double chains. It is extremely important as a catalyst. The catalytic activity may be due to reversible loss or gain of oxygen when heated. All these important applications of the material led us to take up the study of forming nanostructure in this material. The investigation of the development of this nanostructure by line profile analysis by X-ray diffraction (XRD) constituted the main aim of our study.

The basic requirement for a reliable size–strain separation on the basis of WA method is reasonably resolved profiles and proper estimation of the background. Incorrect estimation of the background leads to premature truncation of the profiles and causes a 'hook' effect (negative curvature) in the size-Fourier plot and results in a fictitious size contribution. A very useful alternative to such numerical Fourier transformation is the profile fitting/pattern decomposition technique. In this method an analytical function is used to model the X-ray diffraction profiles. It has been shown in the past that small crystallites often produce a Lorentzian shaped profile and the microstrain distribution of a Gaussian, and consequently the intrinsic profile, which is a convolution of an analytical Voigt function. In our method we have considered a pseudo-Voigt function which gives relatively better flexibility and lesser computation time. The predetermined instrumental function convoluted with a symmetric specimen broadened function along with a linearly varying background is fitted to the experimental X-ray diffraction profiles of V_2O_5 and the parameters related to the intrinsic

*Author for correspondence

profile shape is extracted using an convolutive profile fitting algorithm.

In addition, the determination of the grain/crystallite size distribution of nanocrystalline materials is another important aspect. It is often tedious to determine the size distribution from TEM studies. In our procedure it is possible to obtain a smooth distribution function. We have obtained only the column-length distribution. It can be easily converted to a grain size distribution provided that grain shapes are known.

2. Experimental and data analysis

V_2O_5 powder of 99·6% purity of particle size 0·5 μm from Aldrich, USA was dry ball-milled in Al_2O_3 cretoid with a single Al_2O_3 ball of ~ 1·5 cm in diameter for different lengths of time from 8–250 h in a SPEX 8000 Mixer Mill from Glen Creston Ltd., UK. The violent and complex motion in three mutually perpendicular directions was repeated 1000 times/min. The ball pestles crushed the material by impact.

The X-ray diffraction pattern of the as-milled powder specimen was recorded in a Philips PW1710 diffractometer operating at 35 kV and 20 mA using Ni-filtered CuKα radiation. The data was collected in a step-scan mode with a step size of 0·02°2q and a dwell time varying from 2–10 sec per step to obtain a good signal to noise ratio for a reliable profile fitting application. Polycrystalline defect free Si powders were used for instrumental correction.

The X-ray diffraction line profile was assumed to be a pseudo-Voigt function defined as:

$$\mathrm{pV}(2q) = I_0[hL(2q) + (1 - h)G(2q)], \quad (1)$$

where

$$L(2q) = [1 + \{(2q - 2q_0)/w\}^2]^{-1},$$

and

$$G(2q) = \exp[-(\ln 2)\{(2q - 2q_0)/w\}^2],$$

h is the Lorentzian content, I_0 the intensity maxima of k_{a1} peak, $2q_0$ the Bragg angle, w the half width at half maxima (HWHM). An asymmetric function,

$$A(2q) = \exp[-a\,|(2q - 2q_0)/\cot 2q_0\,|],$$

is also convoluted with the above pV function to include the effect of asymmetry originating at low angles due to axial divergence. The peak parameters for the k_{a2} is related to that of the k_{a1} profile via the relations

$$I_{a2}/I_{a1} = 0{\cdot}5,\ w_{a1} = w_{a2}.$$

The peak position of k_{a2} was related to $2q_0$ by Braggs law.

The above function along with a linearly varying background was fitted to the X-ray diffraction profiles and the parameters related to the profile shape was extracted using an algorithm developed by Enzo *et al* (1988). Another program was written by us in FORTRAN 77 for the Warren–Averbach analysis or simplified integral breadth analysis.

The Fourier transform of a pseudo-Voigt function is given by:

$$F(L) = [(1 - h)(p/\ln 2)^{1/2} \exp(-p^2w^2L^2/\ln 2) + hp \exp(-2pwL)], \quad (2)$$

subsequently the size-strain separation was done on the basis of Warren–Averbach method (Warren 1969).

The column-length distribution function was given according to the double-derivative of the size-Fourier coefficients, F_s and the crystallite size distribution $P_v(L)$ according to Guinier (1963). The corresponding average values of the crystallite sizes were calculated therefrom.

3. Results and discussion

3.1 *X-ray diffraction*

Figure 1 shows the evolution of XRD patterns of the V_2O_5 samples milled for increasing times. Considerable broadening of the XRD lines supplemented by reduction of intensity illustrates the effect of heavy deformation on the milled samples. Both the [100] and [001] direction are affected rapidly for initial hours of milling with least effect in the [110] direction. This indicates easy reduction of crystallite size along the a and c orthogonal axes. However the texture of the sample changes from [001] to [110] after about 32 h of milling. This texture was more pronounced in V_2O_5 milled for 150 h or more wherefrom

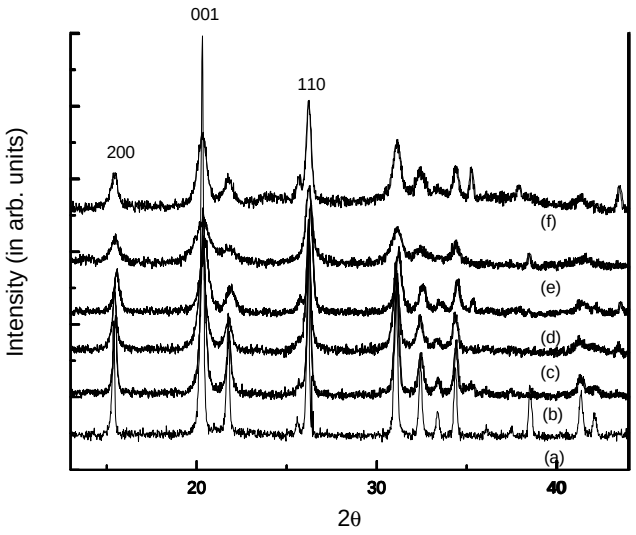

Figure 1. XRD patterns of the milled samples (only a portion is shown) (a) unmilled, (b) 16 h, (c) 32 h, (d) 100 h, (e) 150 h and (f) 250 h. 110 texture is noticed after 32 h of milling.

it was assumed that most crystallites have their [110] planes parallel to the surface of the sample and indicates anisotropic crystallite shape of probably plate like morphology (it can be further substantiated by the fact that in the absence of shape anisotropy of the powder particles such a texture should be barely detectable, as a nearly random arrangement of the powder specimen in the sample holder was expected). The presence of Al_2O_3 peaks was noticed after 32 h of milling which was however, noticeably absent in the samples milled for 150 h and beyond but reappears after 250 h of milling.

3.2 *Lattice parameter*

The lattice parameter measurements however did not indicate considerable contamination of the samples from vial and ball. The values of cell parameters are quoted in table 1.

3.3 *Line broadening analysis*

In our procedure of two-stage analysis, first the profile shape parameter was obtained through a pattern-decomposition followed by a multiple-order Warren–Averbach method for size–strain separation. A qualitative description of operative cause of line broadening is presented on the basis of the variation of the profile shape parameter. Finally the mean strain microstrain and its variation with coherence length was interpreted in terms of local strain and strain derivatives to extract the information regarding the nature of stress confinement in the crystallites.

3.3a *Profile shape analysis*: The variation of average shape parameter Φ (= $2w/b$, $2w$ = FWHM and b = integral breadth) (Langford 1992) with milling times for the (100) and (001) families of reflections are shown in figure 2 (LL, lorentzian limit and GL, gaussian limit). For initial milling times the Lorentzian content of the profile increases rapidly (up to 32 h) indicating the fracture of the powder particles due to repeated ball–powder impact and reflecting the size broadening as an operative cause for overall line-broadening. For longer milling time (t > 32 h) the Gaussian content increased (up to 150 h) with milling time indicating the propensity of strain-broadening. This fact was also supported by the measurements of crystallite size and strain which indicated a pronounced increase in the values of microstrains with relatively less influence on the crystallite size in the intermediate milling times. A further decrease in the shape factor was noticed for samples milled beyond 150 h which indicated further decrease in the crystallite size and relaxation of the lattice microstrains. The shape parameter analysis, therefore, lead to a consistent picture with regard to size and strain effects.

3.3b *Warren–Averbach analysis*: The qualitative arguments on the basis of profile shape analysis was further substantiated by a detailed Fourier line shape analysis within the framework of Warren–Averbach method. The strain corrected size Fourier coefficients obtained from WA analysis as a function of the coherence length, L showed no systematic 'hook' effect for the different milling times indicating the size-broadened profile was predominantly Lorentzian in nature (the presence of gauss component in the size broadened profile however cannot be ruled out). In our analysis all the three available order for [100] direction (200–400–600) was used. The close proximity of the points in the ln A_L vs d^{*2} plot suggest that the effect of higher strain moments ($\langle e^4 \rangle$ etc) might be low and the WA method is fairly reliable and the alternative method of van Berkum *et al* (1994) did not yield any better result. However, for longer milling times the diffuseness and overlapping of the neighbouring peaks impairs the reliability of the pattern decomposition and only two orders were used. The crystallite size along with

Table 1. Variation of lattice parameter with milling time.

Milling time (h)	Lattice parameter (Å)		
	a	*b*	*c*
0	11·5100 (11·51*)	3·5631 (3·559*)	4·3708 (4·371*)
8	11·4551	3·5451	4·3539
16	11·4962	3·5598	4·3679
32	11·5061	3·5623	4·3749
64	11·4959	3·5632	4·3678
100	11·4704	3·5496	4·3619
150	11·4933	3·5606	4·3626
200	11·4857	3·5583	4·3615
250	11·4869	3·5605	4·3751

*Reported value PDF 9-387

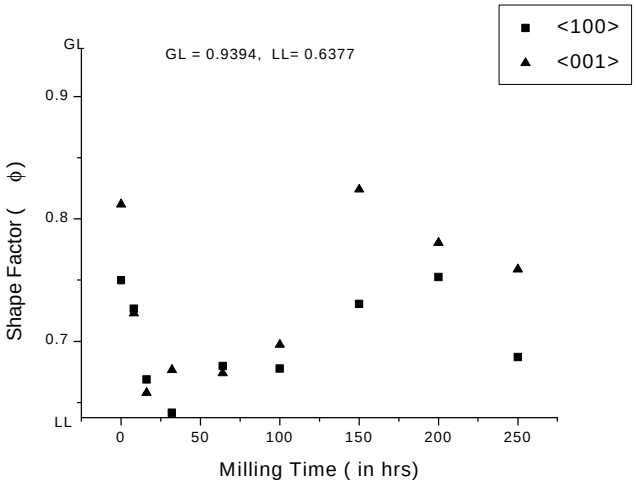

Figure 2. Variation of average shape factor with milling time along two different crystallographic directions.

maximum errors calculated on the basis of WA method is given in table 2. It is evident from table 2 that the crystallite sizes decrease rapidly for initial hours of milling and attained a saturation at higher milling time. The saturation crystallite size was ≈ 10 nm. The difference in the values of the crystallite sizes for the two directions indicated size anisotropy up to about 150 h of milling. However, after 200 h of milling the crystallites assume an isotropic size at least in the above two crystallographic directions. These results are in conformity with the ball-milled metallic samples (Hellstern *et al* 1989; Lutterotti and Gialanella 1997) where a similar behaviour of the crystallite size with milling time was observed, the only difference was the milling time required to attain a saturation crystallite size which was much less in case of metallic samples. However, the meaning of 'crystallite size' should be emphasized at this point. Most of the results available in the literature is either based on the measurements of the integral breadths of the X-ray diffraction lines or TEM measurements (Hellstern *et al* 1989; Eckert *et al* 1992). There is a basic difference in the two approaches, while TEM measures the particle or grain dimensions, X-ray line breadths usually measure the average column length along the crystallographic direction which is assumed to be diffracting coherently within itself and incoherently with respect to the other regions. In the presence of subgrain structures systematic differences between the two measurements exist. Thus X-ray line broadening in conjunction with TEM measurements can give qualitative inference regarding the microstructure of the nanocrystalline materials and the occurrence of a possible plastic deformation during ball-milling.

The volume-weighted crystallite-size (column-length) distribution ($P_v(L)$) for the two different crystallographic directions are shown in figures 3a and b. The distribution function progressively narrowed down with milling time for both the directions [100] and [001]. In some cases humps could be noticed in the distribution function which however did not indicate bimodal size-distribution (as a single pV function cannot model a bimodal size distribution)

Table 2. Crystallite size and r.m.s. microstrain from Warren–Averbach analysis.

	[100]				[001]			
Milling time (h)	D_{eff} (nm) Error ± 1–2 nm	D_v (nm)	$\langle e_0^2\rangle^{1/2}$ × 10^3	$\langle e_L'^2\rangle^{1/2}$ × 10^5	D_{eff} (nm) Error ± 1–2 nm	D_v (nm)	$\langle e_0^2\rangle^{1/2}$ × 10^3	$\langle e_L'^2\rangle^{1/2}$ × 10^5
0	90	113	2·60	1·6	74	84	3·0	7·5
8	20	29	2·95	15·0	26	38	6·3	29·6
16	22	36	4·50	14·8	14	27	5·5	27·7
32	14	25	5·50	28·0	8	14	6·3	42·4
64	12	19	6·32	38·7	8	14	8·4	58
100	11	20	6·30	41·0	10	15	14·5	143
150	12	16	15·50	109·0	7	8	21·6	306
200	10	13	9	72·0	9	11	13.4	138
250	10	14	9	60·0	10	12	11·0	109

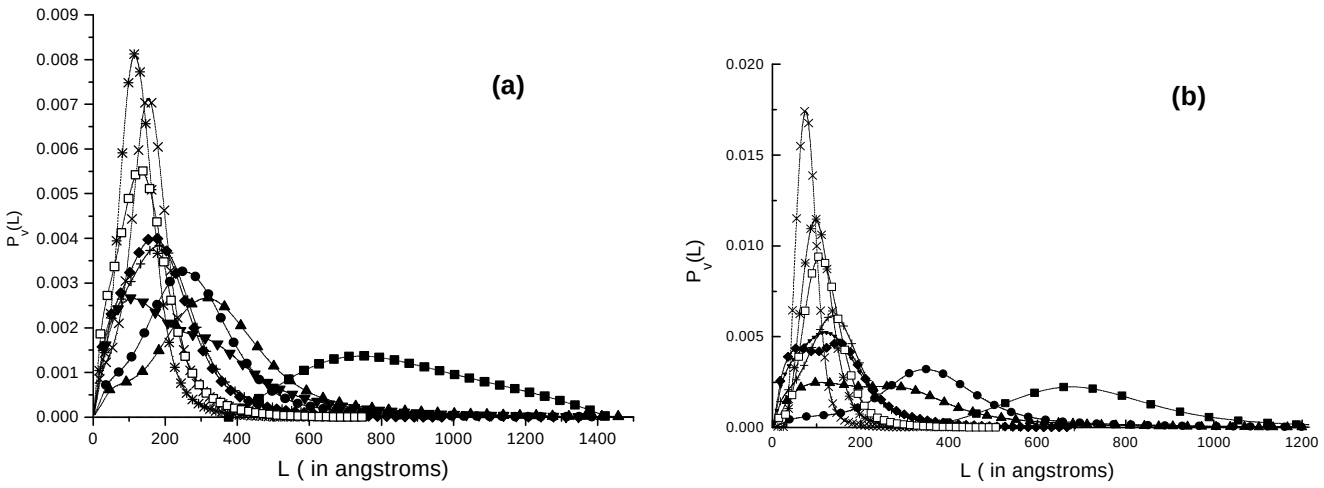

Figure 3. Volume-weighted crystallite size distribution with milling time **(a)** along [100] and **(b)** along [001]; (■ unmilled, ● 8 h, Δ 16 h, ∇ 32 h, ◆ 64 h, + 100 h, × 150 h, ✶ 200 h, □ 250 h).

and was probably due to underestimation of the gaussian content of the lower order peaks. For the longest milling time achieved a narrow distribution indicated a trend towards isotropic crystallite size. The value of the volume weighted crystallite size, D_v was obtained from the $A_s(L)$ curve according to the equation

$$D_v = 2\int A_s(L)\,dL, \tag{3}$$

and is given in table 2. Since the error in the $A_s(L)$ curve will be magnified in the $P_v(L)$ due to the double differentiation involved, $D_v(L)$ was not calculated from the distribution function $P_v(L)$. The volume weighted crystallite size also decreased with the milling time. Discrepancies in some cases was due to uncertainty in the size-Fourier coefficients. The ratio D_v/D_{eff} for milling times < 100 h was less than but close to 2 indicating that the size broadened profile was in general Voigt in nature with more weight towards Lorentzian content (Balzar and Ledbetter 1993) (for purely Lorentzian size broadened profile the value is exactly 2 and the distribution function $P_v(L)$ could be approximated by a log-normal distribution). Further it was observed that for milling times up to 32 h the ratio increased and the distribution function indicated an increased fraction of smaller crystallites establishing that the operative cause of overall line broadening for milling times < 32 h was size broadening. The distribution function beyond 32 h did not indicate any measurable change in the fraction of smaller crystallite up to about 100 h of milling. The above ratio, however, decreased after 100 h of milling and reached near the value of an ideal gaussian size broadened profile. A subsequently narrow distribution indicated that the ball-milled samples had achieved an almost uniform size distribution. Along [001] the distribution was narrowest for 150 h sample and thereafter widened gradually with an increasing fraction of larger crystallites (see the tail of the distribution) and a small concomitant shift in the maxima suggested small recovery effect and a small strain relaxation. Along [100], however the narrowest distribution was achieved after 200 h milling and small broadening occurred, thereafter the average value remained the same within error limits. The deformation characteristics was therefore different in the two different crystallographic directions beyond 150 h of milling. The variation of internal strains measured with the coherence lengths calculated on the basis of WA analysis is shown in figures 4a and b. Although a gaussian strain distribution for which the WA analysis yields exact results indicates that the rms microstrains should not vary with the coherence length, but often the rms microstrains obtained from the WA analysis increases rapidly for small values of L. It was observed from figure 6 that for lower milling time (t < 32 h) the variation was not significant but beyond 32 h significant variation could be observed. The interpretation of the decrease of mean square strain (MSS) with L in terms of localized strain fields was supported by calculations of MSS in terms of dislocation and spatial arrangement of dislocation (Wilkens 1962, 1979; Rothman and Cohen 1971). Although such simulations indicate that WA method overestimates the decrease of $\langle e_L^2 \rangle$ with L, still the decrease may be physically interpreted in terms of local strain $\langle e_0^2 \rangle$ and their derivatives to understand the nature of strain fields (Turunen *et al* 1983).

Defining $\langle e_L^2 \rangle$ as

$$\langle e_L^2 \rangle = \left\langle \left[\frac{1}{L} \int_{-L/2}^{+L/2} E(x)\,dx \right]^2 \right\rangle, \tag{4}$$

where $x = z - z_0$, z is the coordinate in the crystal space and z_0 the middle point of each range of length, L in a column, $E(x)$ was the normal strain and $e(z)$ the local strain in terms of the actual coordinate z in the interval $-L/2 \le x \le L/2$, $E(x) = e(z - z_0)$. Performing the above integration after expanding $E(x)$ in a Taylor's series and subsequent averaging over all possible values of z_0 the following expression for the mean square strain was

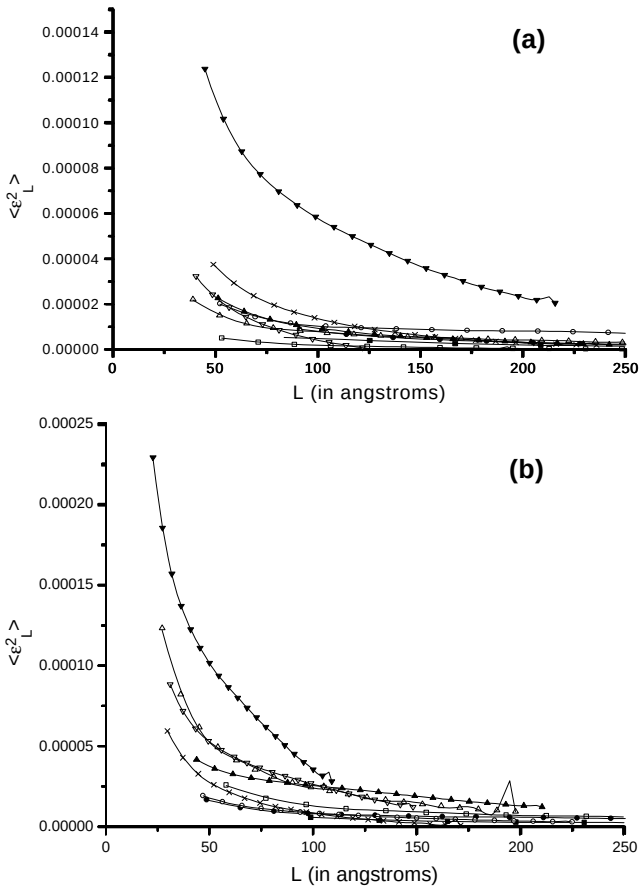

Figure 4. Variation of mean square strain with milling time. Results of polynomial fitting. **(a)** [100] and **(b)** [001] (■ unmilled, □ 8 h, ● 16 h, ○ 32 h, Δ 64 h, Δ 100 h, ▼ 150 h, ∇ 200 h, × 250 h).

obtained on the basis of assumption of randomness of strains at the column ends

$$\langle e_{\mathrm{L}}^2\rangle = \langle e(z)^2\rangle - \frac{1}{12}\langle e'(z)^2\rangle L^2 + \frac{1}{360}\langle e''(z)^2\rangle L^4 - \frac{1}{20160}\langle e'''(z)^2\rangle L^6 \cdots \quad (5)$$

The above equation was fitted to the mean-square microstrain curves with a total of 12 parameters. The fitting range was selected by inspecting the volume-weighted column-length distribution function to include the maximum possible column-length in the fitting process. A Marquardt–Levenberg fitting algorithm was used. The fitted coefficients were alternatively negative and positive in accordance with the above series expansion. The local mean square strain and mean square strain derivatives are given in table 2. Only the first derivative was given which is often sufficient to explain the results. Figures 5a and b give the variation of the local mean square strains and the mean square strain derivatives with milling time. It is clear from table 2 that the strains vary rather anisotropically with milling time in different crystallographic direction.

Along [001] the local mean-square strain varied rather slowly at smaller milling time (t < 32 h). In the same range the volume-weighted crystallite size decreased rapidly (see $1/D_v$ vs t plot in figure 5b). Beyond 32 h the local strain increased rapidly and reached a maximum of ~ 2% at 150 h and thereafter decreased (figure 5b). Similar nature was observed for the mean square derivative,

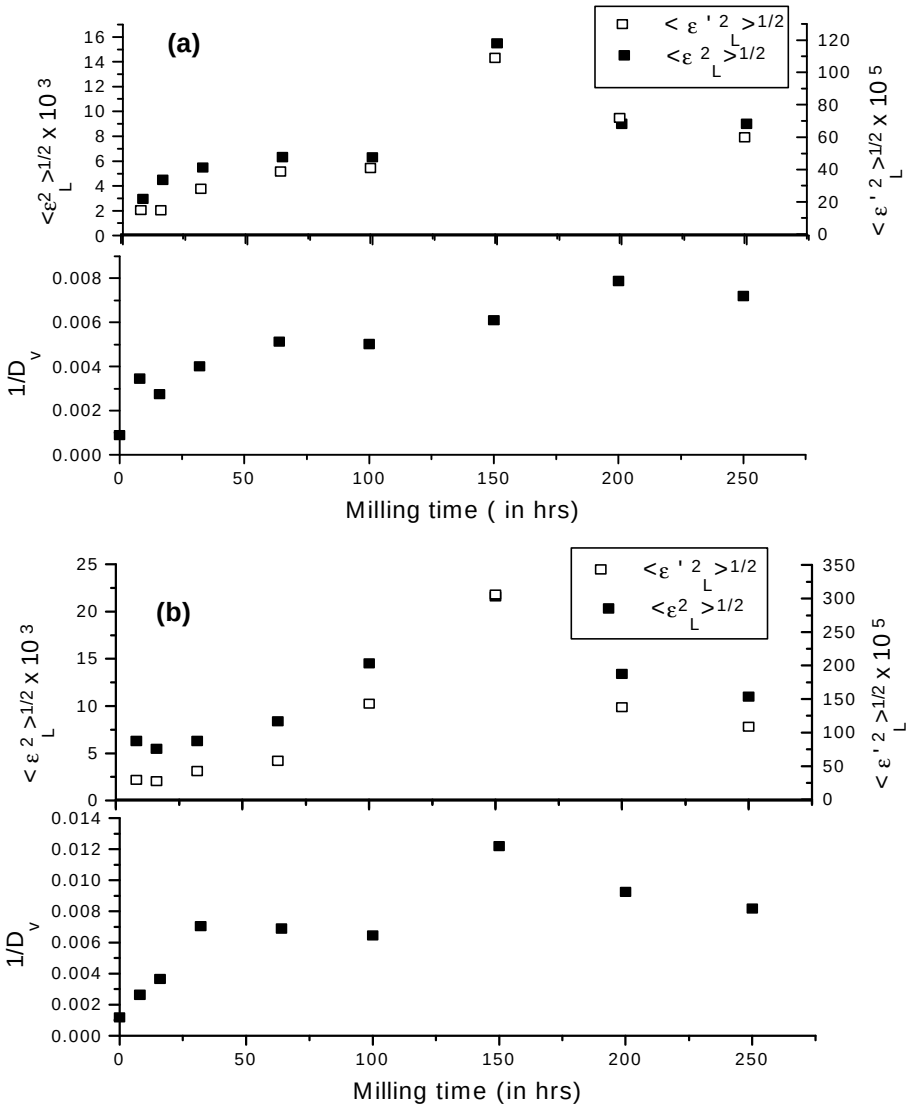

Figure 5. Variation of local mean square strains, strain derivative and inverse of volume-weighted crystallite size D_v (Å^{-1}) with milling time **(a)** [100] and **(b)** [001].

indicating an increased non-uniformity in the column strain with milling time. Such a behaviour along with a similar nature of the crystallite size distribution (no significant increase in the fraction of smaller crystallites) suggests that further fracture was inhibited and the crystallite interfaces increasingly contributed to the lattice strains with increased localization of the stress fields. The decrease in the microstrain and strain derivatives beyond 150 h indicated a relaxation of strain as predicted in an earlier paragraph. Similar behaviour was observed along [100] (figure 5a) where the local strains and mean square strain derivatives increased monotonically with milling time and reached a maxima for 150 h milled sample and decreased thereafter.

The crystallite size also decreased monotonically and increased slightly after 250 h of milling. The behaviour of crystallite size and strain along [001] and [100] after 150 h was thus significantly different and could only be explained in terms of a change in the crystallite morphology. It was interesting to note that the level of plastic strain was similar to that often found in heavily deformed metallic samples (Hellstern *et al* 1989; Wagner *et al* 1996). Measurement of lattice parameters provided a too small value of $\Delta a/a$ or $\Delta c/c$ and was not consistent with the microstrain measurements.

The above results presented for ball-milled V_2O_5 sample was not consistent with that of ball-milled metallic samples where the root-mean square microstrains increase rapidly during initial hours of milling due to large increase of dislocation densities to a saturation value as the material assumes nanocrystalline dimension. Here it is assumed that the energy supplied by ball-milling is not sufficient for dislocation motion and hence further grain refinement (Hellstern *et al* 1989). Although the nature of rms microstrains with milling times are different the variation of mean square strain with coherence length, L is similar for both metallic and ceramic nanocrystals (Wagner *et al* 1996; Lutterotti and Gialanella 1997; Reimann and Wurschum 1997). A general conclusion could be derived from such results that crystallite or grain boundaries are disordered. Although HREM studies indicate that the grain boundary structure is different for metals and oxides, disordered boundary structure has been observed both in metallic (Thomas *et al* 1990; Wunderlich *et al* 1990; Valiev and Musalimov 1994) as well as oxide nanocrystals (Rickerby 1997). It has also been observed that epitaxial grain boundary tend to occur less frequently in oxides than in metals (Ishida *et al* 1995). Presence of shear defects in nanocrystalline TiO_2 (Chang *et al* 1993) has also been found in the grain boundary regions and was explained as due to oxygen deficiency. In all cases the width of the disordered region is small and extends up to a few nanometers only. Such a short-range disordered region was actually observed in the present case where the strain variation occurred mostly up to 8–10 nm. Thus X-ray line broadening study in terms of microstrains provided an alternative and indirect way to study the extent of inhomogeneity in nanocrystalline materials.

4. Conclusions

From the present study the following conclusions were made:

(I) Ball-milling of V_2O_5 powder lead to the formation of nanocrystalline powders along with significant amount of plastic inhomogeneous strains.
(II) The initial hours of milling lead to considerable grain refinement ($t < 32$) whereas microstrains were the prominent cause of line broadening at higher milling times.
(III) Nature of variation of microstrains with the coherence length was similar to that obtained for metals. Increasing local strain and strain gradients in the diffracting columns with milling time indicated spatial confinement of stress fields and disorder in a narrow region probably along the crystallite interfaces.
(IV) Size anisotropy along [001] and [100] exists up to 150 h of milling and a [110] texture was observed from the X-ray diffraction pattern along with broad size distribution. However, a narrow distribution of crystallite size after 150 h of milling and isotropic crystallite size along both the [001] and [100] were apparent.

References

Balzar D and Ledbetter H 1993 *J. Appl. Cryst.* **26** 97

Chang W, Cosandey F and Hahn H 1993 *Nanostruc. Mater.* **2** 29

Eckert J, Holzer J C, Krill C E and Johnson W L 1992 *J. Mater. Res.* **7** 1751

Enzo S, Fagherazzi G, Benedetti A and Polizzi S 1988 *J. Appl. Cryst.* **21** 536

Guinier A 1963 *X-ray diffraction* (San Francisco: Freeman)

Hellstern E, Fecht H J, Fu Z and Johnson W L 1989 *J. Appl. Phys.* **65** 305

Ishida Y, Ichinose H, Kizuka T and Suenaga K 1995 *Nanostruc. Mater.* **6** 115

Langford J I 1992 *Accuracy in powder diffraction II* (eds) E Prince and J K Stalik (Washington: US Department of Commerce) p. 110

Lutterotti L and Gialanella S 1997 *Acta Mater.* **46** 101

Reimann K and Wurschum R 1997 *J. Appl. Phys.* **81** 7186

Rothman R L and Cohen J B 1971 *J. Appl. Phys.* **42** 971

Rickerby D G 1997 *Philos. Mag.* **B76** 573

Rubin Aita C, Li Liu Y, Kao M L and Hansen S D 1986 *J. Appl. Phys.* **60** 749

Thomas G J, Siegel R W and Eastman J A 1990 *Scr. Metall. Mater.* **24** 201

Turunen M J, de Keijser Th H, Delhez R and van de Pers N M 1983 *J. Appl. Cryst.* **16** 176

Valiev R Z and Musalimov R Sh 1994 *Phys. Met. Metall.* **78** 666

van Berkum J G M, Vermeulen A C, Delhez R, de Keijser Th H and Mittemeijer E J 1994 *J. Appl. Cryst.* **27** 345

Wagner C N J, Yang E and Boldrick M S 1996 *Nanostruct. Mater.* **7** 1

Warren B E 1969 *X-ray diffraction* (Reading, Mass: Addison Wesley)

Wilkens M 1962 *Phys. Status Solidi* **2** 693

Wilkens M 1979 *J. Appl. Cryst.* **12** 119

Wunderlich W, Ishida Y and Maurer R 1990 *Scr. Metall. Mater.* **24** 403

Yong-Su Oh, Yuichi Watanabe and Masasuka Takata 1992 *J. Ceram. Soc. Jap.* **100** 1390